strate. Among several possible ways for weighting the grating coupling coefficient, we adopted changing the thickness of cladding layer. By using the holographic exposure technique, the grating mask was produced on a 300 nm-thick cladding layer, part of which was etched to the thickness of 260 nm. The Bragg reflectors with weighted coupling coefficients were successfully fabricated by CHF_3 reactive ion etching. Through SEM observation, the depth of grating was found to be 60 nm. It can be concluded by the calculation that the desired coupling coefficients of 50 cm^{-1} and 30 cm^{-1} are obtained for the cladding thicknesses of 300 nm and 260 nm, respectively.

1. H. M. Gibbs, S. S. Tarng, J. L. Jewell, D. A. Weinberger, K. Tai, A. C. Gossard, S. L. McCall, A. Passner, W. Wiegmann, Appl. Phys. Lett. **41**, 221–222 (1982).
2. J. Yumoto, S. Fukushima, K. Kubodera, Opt. Lett. **12** (10), 832–834 (1987).
3. P. Li Kam Wa, P. N. Robson, J. P. R. David, G. Hill, P. Mistry, M. A. Pate, J. S. Roberts, Electron. Lett. **22** (21), 1129–1130 (1986).
4. K. Shimomura, H. Murata, M. Izutsu, T. Sueta, J. J. Appl. Phys. **32** (6B), L840–L842 (1991).

CThI84

Optically controlled quantum well light modulator

N. T. Pelekanos, B. Deveaud,* P. Gravey, F. Clérot, J. M. Gérard,** J. Hebling,*** J. Kuhl,*** *France Télécom, CNET-Lannion, BP 40, 22301 Lannion, France*

In this report, we present preliminary results on a light modulator based on the Quantum Confined Stark Effect (QCSE)[1] but for the first time operating all-optically. The principle of operation of the device is as follows: every period of the heterostructure contains three quantum wells (QWs) designed in such a way that following above band-gap photoexcitation a large fraction of the photogenerated electrons and holes tend to separate and accumulate in the exterior QWs, creating a local space-charge field having its maximum in the region in between and acting via the QCSE on the exciton resonance of the central QW.

In Fig. 1, we show a schematic band diagram of one period of the heterostructure. The samples studied here contain typically 25 periods. The three QWs are enumerated from left to right. QW1 is ≈25 Å of GaAs, surrounded typically by a graded (Al,Ga)As (x = 36 – 42%, 800 Å) and an AlAs barrier (100Å). The combination of a narrow GaAs QW adjacent to an AlAs layer is the key aspect of the device. Following photoexcitation above the AlGaAs barriers or QW1 ($\lambda_{write} \leq 620$ nm or 700 nm at T = 300 K, respectively), this layer combination functions as a one-way "quantum filter" for the photocarriers of QW1, by blocking the holes out but allowing the electrons to transfer rapidly into QW2. This is due to the fact that, for sufficiently thin GaAs layer thicknesses, the electron energy level at the Γ-point in the GaAs QW is higher than the one at the X-point in the AlAs layer. Γ –

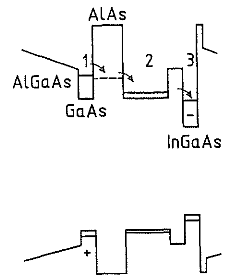

CThI84 Fig. 1. Schematic of one period and photogeneration of electric field by rapid electron transfer from QW1 to QW3. The QW energy levels at the Γ point are denoted by full lines whereas the X point energy level in the AlAs layer by a dotted line.

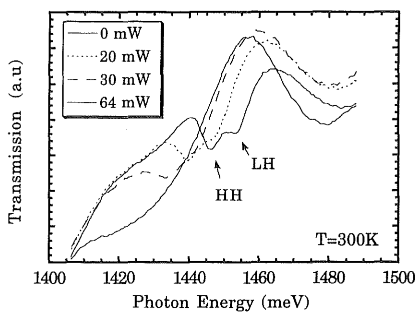

CThI84 Fig. 2. Transmission spectra in the region of the QW2 exciton for various power levels of the coincident Krypton laser. For our focusing conditions, 1 mW corresponds approximately to 0.5 W/cm^2.

X electron transfer times in the subpicosecond regime have been measured in thin GaAs/AlAs superlattices.[2] QW2 is 150 Å of GaAs and QW3 80 Å of (In,Ga)As (x = 10%). The electrons that pass through the quantum filter leaving behind holes, are able to subsequently tunnel through a thin (≤50 Å) (Al,Ga)As barrier into QW3. The resulting space-charge electric field acts upon the excitonic resonance of QW2 ($\lambda_{read} \approx 860$ nm at T = 300 K).

In Fig. 2, we show the room temperature transmission spectra of one of our samples in the region of the QW2 exciton, for various power levels of a coincident CW Krypton laser operating at 647 nm. For our focusing conditions, 1 mW corresponds approximately to a power density of 0.5W/cm^2. The distinct heavy (HH) and light hole (LH) exciton features, indicated by arrows on the reference transmission trace, clearly redshift under the effect of illumination. In addition, the exciton features smear out with increasing laser power, consistent with the electric-field-induced exciton broadening and decrease in oscillator strength observed in QCSE experiments.[1] The maximum transmission change observed is around 30%, corresponding well to the estimated value by simply considering 25 times 1% absorption per active QW. In Fig. 3, we plot the exciton energy position as a function of Krypton laser power. We measured a redshift of about 20 meV

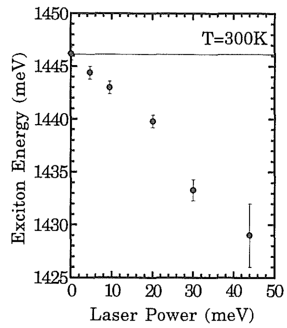

CThI84 Fig. 3. Redshift of the QW2 exciton resonance with increasing power of coincident Krypton laser.

with optical excitation of the order of 20 W/cm^1. This redshift corresponds for a 150 Å QW to an effective electric field across the active QW of nearly 50 kV/cm,[3] which is sufficient for many device applications. Ongoing work is focusing on optimizing the structure parameters and understanding the dynamics of this device. The all-optical operation of this modulator in conjunction with the low switch-on power densities are very appealing for applications in the area, for example, of ultrafast parallel image processing.

Presently: Ecole Polytechnique Lausanne, CH 1015 Lausanne, Switzerland.
***France Télécom, CNET-Bagneaux, BP 107, 92225 Bagneux, France*
****Max-Planck-Institut für Festkörperforschung, Heisenbergstr. 1, 70569 Stuttgart, Germany*

1. D. A. B. Miller, D. S. Chemla, T. C. Damen, A. C. Gossard, W. Wiegmann, T. H. Wood, C. A. Burrus, Phys. Rev. B **32**, 1043 (1985).
2. J. Feldmann, J. Nunnenkamp, G. Peter, E. Göbel, J. Kuhl, K. Ploog, P. Dawson, C. T. Foxon, Phys. Rev. B **42**, 5809 (1990).
3. L. Vina, E. E. Mendez, W. Wang, L. L. Chang, L. Esaki, J. Phys. C. Solid State Phys. **20**, 2803 (1987).

CThI85

An approach to visual cortex operation: optical neuron model

J. A. Martín-Pereda, A. González-Marcos,* *E.T.S. Ingenieros Telecomunicacion. U.P.M., Universidad Politecnica De Madrid, Ciudad Universitaria, 28040 Madrid, Spain*

Several works have been published in the last years concerning the modelling and implementation of the visual cortex operation. Most of them present simple neurons with just two different responses, namely inhibitory and excitatory. Some of the different types of visual cortex cells are simulated in these configurations.

Another approach is going to be reported in this paper. Based on a previously reported logic cell structure,[1,2] the five types of cells present at the vertebrate retina and their intracellular response, as well as their connections with each other, have been simulated. The main scheme of our configuration is shown in Fig. 1. As in the visual cortex,

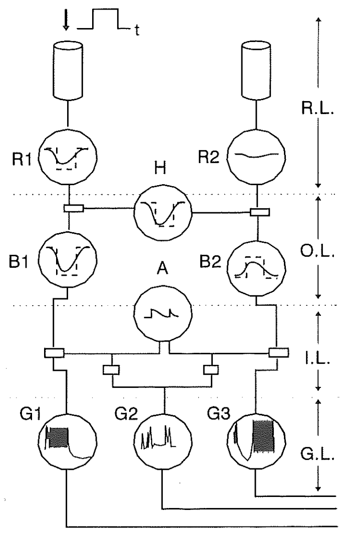

CThI85 Fig. 1.

it is divided into four layers: receptor, outer, inner, and ganglion cell layers. These four layers are composed by five different cell types: receptor (rod and cones), bipolar, horizontal, amacrine, and ganglion cells. These five cells have been implemented with our previously reported Optical-Processing Element.

As it has been shown, our structure is able to process two optical input binary signals, being the output two logical functions. The type of processing is related to the eight main Boolean Functions. According to the value of two external control signals, any one of these functions can be obtained from the structure. Moreover, if a delayed feedback from one of the two possible outputs to one or both of the inputs is introduced, a very different behaviour is obtained. Depending on the value of the time delay, an oscillatory output can be obtained from a constant optical signal input. Period and length pulses are depending on delay values, both external and internal.

With the above considered facts, a configuration similar to the one proposed by Dowling[3] to summarize the activity of the various retinal cells has been implemented. As it can be seen, the receptor on the left is illuminated with a brief flash of light imposed on a dim background, which illuminates both receptors, R_1 and R_2. Their control signals make them to operate with NAND functions. Same function is performed by the horizontal cell H. Bipolar cells, B_2 and B_2, operate as AND or NAND functions according to the control signals imposed by the previous layer.

Another type of function is performed by the amacrine cell. It gives a periodic signal, with period and pulse length depending on the characteristics of the signals coming from the bipolar cells. The composite signals from bipolar and amacrine cells arrive to the ganglion cells from where the final signal is obtained. In the studied case, three are the outputs. The first one is a train of light pulses being its length the same one as the input flash. The third one is always a sequence of short pulses; only when it was light at the input, pulses disappear. Finally, the second one gives a very short train of pulses at the beginning and at the end of the initial flash.

Our configuration has been implemented, partly, with optoelectronic techniques. A computer simulation has given us the behaviour of the whole cell. Its applications can go from edge to moving objects detection.

*Departamento de Automática, Universidad De Alcala De Henares, 28871 Alcala De Henares, Madrid, Spain

1. A. González-Marcos, J. A. Martín-Pereda, "Quasi-chaotic digital behaviour in an optically processing element," SPIE **2038**, 67–77 (1993).
2. J. A. Martín-Pereda, A. González-Marcos, "Optical Programmable Processing Element using Optical Fibers," IEEE Lasers and Electro-Optics Society, LEOS'92. Boston, November, 1992, p. 15–20.
3. Dowling, J. E. "Organization of the vertebrate retinas" Investigative Ophthalmol. **9**, 655–680 (1970).

CThI86

Ultrafast erasable optical storage in Sb-Rich GeSb films

C. N. Afonso, J. Solis, M. C. Morilla, M. A. Ollacarizqueta, *Instituto de Optica, CSIC, Serrano 121, 28006 Madrid, Spain*

Phase change optical storage is the most promising alternative to magneto-optical recording. This technology is an all-optical one and has a much better signal to noise ratio and a simpler reading mechanism that simplifies the optical head. This leads to a decrease in the access time and to make the phase change disks interchangeable with the earlier optical storage products, the CDROM and WORM discs. The most significant drawback with phase-change materials has been the need for materials with high-speed crystallization, crystallization triggered by <100 ns laser pulses being usually required.

The aim of this work is to demonstrate that micron-sized bits can be recorded with 12 ns in Sb-rich GeSb films. It will be also shown that reversible phase changes (amorphous ⇆ crystalline) can be produced by irradiation with ps pulses of different energy density.

Laser irradiations are performed by means of 12 ns pulses from an intra-cavity modulated Ar^+ laser focused to the sample to a 1/e beam radius of 4 μm and 10 ps pulses from an amplified, synchronously pumped dye laser focused to 100 μm. A He-Ne probe beam is focused in all cases at the centre of the irradiated area, the 1/e beam radius being of 1.7 μm in the former case. The probe beam is used to measure in real time the reflectivity changes in order to follow the process kinetics and determine the transformation times. The samples are amorphous $Ge_{0.13}Sb_{0.87}$ films sputtered deposited onto glass and carbon-coated mica substrates.

The results show that 1.5 μm sized bits are recorded with 12 ns pulses, the recording process being completed within tens of nanoseconds. Optical and structural images of hundred μm areas irradiated with pulses of 10 ps show clearly that phase reversal can be achieved by alternating ultrashort pulses of different energy density. The reflectivity transients show that the transformation process is also completed within the ns time scale. The formation of an extended solid solution upon crystallization explains the fast transformation process in addition to the high optical contrast. The physical mechanism, which controls the reversibility of the fast structural transformation, is found to be related to the dependence of the degree of undercooling achieved prior to solidification on the energy density.

CThI87

Erasable zone plate in bacteriorhodopsin film for photonic switching

Y. Okada-Shudo, K. Ujihara, H. Tomioka,* I. Yamaguchi,** *Department of Electronics Engineering, University of Electro-Communications, 1-5-1 Chofugaoka, Chofu-shi, Tokyo, 182, Japan*

The photochromic protein bacteriorhodopsin (bR), which is related to the human visual pigment, is found in the purple membrane of *Halobacterium halobium* in two-dimensional crystallized form. The absorption of a visible photon by bR triggers a photocycle as shown in Fig. 1. Both the forward and reverse photoreactions produce stable products in less than 3 picoseconds at 77 K. Its photochromic properties, i.e., the light-driven reversible color changes, are used in real-time holographic recording.

Figure 2 shows schematic diagram of the principal components of an erazable optical storage medium of a bR based photonic switching. The bR film is embedded in acrylamide filling a glass cell. Its size is 1 cm × 1 cm × 500 μm and an initial optical density at 570 nm of OD = 1.2. To increase light sensitivity, M lifetime is prolonged by the addition of guanidine hydrochloride about 100 milliseconds. The arrangement employed to obtain the Fresnel zone plate is a Mach-Zehnder interferometer, using one of the lines (λ = 515 nm) of an Ar^+ laser. In one

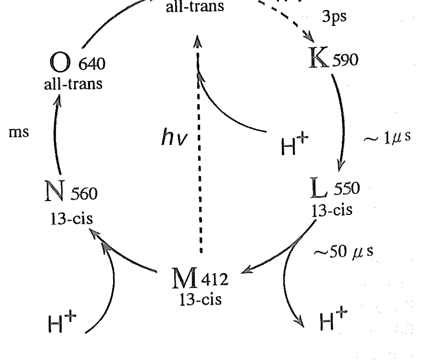

CThI87 Fig. 1. Scheme of the photochemical and thermal conversions of bR. The photointermediates are abbreviated by single letters. Index numbers indicate the absorption maxima. In this case the photochemical transition bR → M is used for hologram formation.